

Antenna Feedhorn Software Upgrade

P. D. Potter
Radio Frequency and Microwave Subsystems Section

The HYBRIDHORN computer program was developed in 1973 to serve as an item of general purpose antenna feedhorn design and analysis software, and has been utilized extensively since that time for this purpose. The 1973 formulation contains a small flare angle approximation which is subject to question for designs such as the Williams S- and X-band feedhorn. Additionally, the original formulation did not allow azimuthal variation indices other than unity. The HYBRIDHORN program has been recently upgraded to correct both of these deficiencies. A new large flare angle formulation has been found which appears to have escaped the attention of others. In the upgrade, all of the major program elements have been converted to Univac 1108 compatible structured Fortran (SFTRAN) for ease of software maintenance. This article describes the small and large angle formulations and presents some sample numerical results.

I. Small Flare Angle Formulation

The small flare angle approximation is discussed in Ref. 1. The formulation is based on the fact that the fields on a spherical cap in the horn aperture are well approximated by the standard cylindrical (Bessel function) fields (Ref. 2).

Figure 1 shows the horn geometry. Clarricoats (Ref. 3) derived the cylindrical fields for the case of arbitrary index, m , of azimuthal variation. For linear polarization, the following field expressions apply in the horn flare:

$$E_{rmm} = + E_{mn} \cdot J_m(x) \sin(m\phi) \quad (1a)$$

$$H_{rmm} = - \left(\frac{E_{mn}}{Z_0} \right) \cdot \text{BAL}_{mn} \cdot J_m(x) \cos(m\phi) \quad (1b)$$

$$E_{\theta mn} = - j E_{mn} \cdot \left(\frac{k}{K_{mn}} \right) \cdot \left[\frac{J_m(x)}{x} \right] \cdot \left[\beta_{mn} F_m(x) + m \text{BAL}_{mn} \right] \sin(m\phi) \quad (1c)$$

$$E_{\phi mn} = -jE_{mn} \cdot \left(\frac{k}{K_{mn}}\right) \cdot \left[\frac{J_m(x)}{x}\right] \cdot \left[m + \bar{\beta}_{mn} + \text{BAL}_{mn} \cdot F_m(x)\right] \cos(m\phi) \quad (1d)$$

$$H_{\theta mn} = +j \left(\frac{E_{mn}}{Z_0}\right) \cdot \left(\frac{k}{K_{mn}}\right) \cdot \left[\frac{J_m(x)}{x}\right] \cdot \left[m + \bar{\beta}_{mn} + \text{BAL}_{mn} \cdot F_m(x)\right] \cos(m\phi) \quad (1e)$$

$$H_{\phi mn} = -j \left(\frac{E_{mn}}{Z_0}\right) \cdot \left(\frac{k}{K_{mn}}\right) \cdot \left[\frac{J_m(x)}{x}\right] \cdot \left[F_m(x) + m + \bar{\beta}_{mn} + \text{BAL}_{mn}\right] \sin(m\phi) \quad (1f)$$

where

$$F_m(x) \equiv x \cdot \left[\frac{J'_m(x)}{J_m(x)} \right] \quad (2)$$

$J_m(x)$ = Bessel function of the first kind and order m

$J'_m(x)$ = derivative of $J_m(x)$ with respect to x

k = free-space propagation constant

Z_0 = free-space characteristic impedance

$$x \equiv K_{mn} \cdot r \cdot \theta \quad (3)$$

$$\bar{\beta}_{mn} \equiv \left(1 - \frac{K_{mn}^2}{k^2}\right)^{1/2} = \text{normalized propagation constant} \quad (4)$$

The assumed circumferential grooves in the horn wall require that the azimuthal electric field components be zero at the wall surface. Thus, from Eq. (1d),

$$\text{BAL}_{mn} = -m \cdot \frac{\bar{\beta}_{mn}}{F_m(x_1)} \quad (5)$$

where

$$x_1 \equiv K_{mn} \cdot r \cdot \theta_1 \quad (6)$$

BAL_{mn} is the mode balance; at the balance frequency it is +1 for the normally-used HE_{mn} modes and -1 for the EH_{mn} modes. At the balance frequency, the horn wall presents infinite longitudinal reactance ($E_{r'mn}$ divided by $H_{\phi mn}$) and radiation patterns result which have essentially equal E - and H -plane patterns.

By consideration of the boundary conditions, the characteristic equation, which may be solved for K_{mn} , is obtained as:

$$F_m^2(x_1) - m^2 \bar{\beta}_{mn}^2 - \left(\frac{K_{mn}}{k}\right)^2 \cdot F_m(x_1) \cdot S_m(x'_1, x'_0) = 0 \quad (7)$$

where

$$S_m(x'_1, x'_0) = \text{radial line admittance function} \equiv x'_1 \cdot \left[\frac{J'_m(x'_1) \cdot Y_m(x'_0) - J_m(x'_0) \cdot Y'_m(x'_1)}{J_m(x'_1) \cdot Y_m(x'_0) - J'_m(x'_0) \cdot Y_m(x'_1)} \right] \quad (8)$$

$Y_m(x)$ = Bessel function of the second kind and order m

$Y'_m(x)$ = derivative of Y_m with respect to x

$$x'_1 = k \cdot r \cdot \theta_1 \quad (9)$$

$$x'_0 = x'_1 + k \cdot \text{GROOVE} \quad (10)$$

GROOVE = groove depth

An important special case of the above equations is that in which the groove depth approaches zero, i.e., the horn has smooth walls. For this case BAL_{mn} either approaches a positive zero, and HE_{mn} modes become TM_{mn} modes, or BAL_{mn} approaches a negative infinity and EH_{mn} modes become TE_{mn} modes. The smooth wall case is thus easily accommodated by the above equations.

The final desired outputs of the HYBRIDHORN program are the E - and H -plane polar radiation patterns, given the frequency of operation, horn geometrical parameters and mode excitation amplitudes and phases. By circular symmetry and resulting orthogonality, the azimuthal radiation pattern dependence is given by the selected order, m , of the sinusoidal/cosinusoidal variation. The following steps are performed to compute the radiation patterns:

- (1) Given the throat region mode phases, the aperture mode phases are determined by numerical solution of (7) at points in the horn flare and numerical integration of β_{mn} .
- (2) The aperture cap fields are determined from Eq. (1c) and Eq. (1d).
- (3) The radiated far-fields are determined by a near-field spherical wave expansion (SWE) about the horn vertex of the aperture cap fields (external fields assumed zero).
- (4) The SWE fields are normalized and phase-translated to a specified reference point on the horn axis.

Equations (1a-1f) are formal solutions to Maxwell's equations in cylindrical coordinates with the assumed anisotropic wall boundary condition; for this cylindrical solution, x is the radial coordinate times K_{mn} . In 1963 Ludwig (Ref. 4) showed that for a spherical geometry such as the horn flare, Eqs. (1a-1f) closely approximate the true fields if the radial cylindrical coordinate is replaced by the arc length (see Eq. (3), (6) and (9) above). This approximation, valid for small flare angles such as those typically utilized in a Cassegrain antenna feedhorn, was discussed in detail by Narasimhan and Rao (Ref. 2). This approximation was used in the original HYBRIDHORN formulation (Ref. 1) and has shown good agreement with experimental data for small (less than 20 degrees) flare angle horns. One of the purposes of the HYBRIDHORN upgrade was to provide the capability of accurate large flare angle calculations. This more rigorous formulation is described in the following section.

II. Large Flare Angle Formulation

The allowable fields in an infinite conical waveguide follow directly from Maxwell's equations. In a source-free isotropic region and assuming $e^{j\omega t}$ time dependence, Maxwell's equations are:

$$\mathbf{E} = \frac{1}{j\omega\epsilon} \cdot (\nabla \times \mathbf{H}) \quad (11a)$$

$$\mathbf{H} = \frac{1}{j\omega\mu} \cdot (\nabla \times \mathbf{E}) \quad (11b)$$

$$\nabla \cdot (\mu H) = 0 \quad (11c)$$

$$\nabla \cdot (\epsilon E) = 0 \quad (11d)$$

Since divergence (curl) is identically zero, from Eq. (11c) H may be expressed as the curl of a vector (known as the vector potential), A_E :

$$H_E \equiv \left(\frac{1}{\mu}\right) \cdot (\nabla \times A_E) \quad (12a)$$

Equating (11b) and (12a), and recognizing that curl (grad) is identically zero, the result is:

$$E_E \equiv -\nabla \phi_E - j\omega \cdot A_E \quad (12b)$$

where ϕ_E is known as the scalar potential.

Similarly, using Eq. (11a) and (11d),

$$E_H \equiv -\left(\frac{1}{\epsilon}\right) \cdot (\nabla \times A_H) \quad (13a)$$

$$H_H \equiv -\nabla \phi_H - j\omega A_H \quad (13b)$$

By combining Eq. (12a) and (12b) with (11a), and Eq. (13a) and (13b) with (11b), the two vector wave equations are obtained:

$$\nabla \times \nabla \times A_E + j\omega \mu \epsilon \nabla \phi_E - k^2 \cdot A_E = 0 \quad (14a)$$

$$\nabla \times \nabla \times A_H + j\omega \mu \epsilon \nabla \phi_H - k^2 \cdot A_H = 0 \quad (14b)$$

As particular solutions of (14a) and (14b), consider E - (TM) and H - (TE) waves:

$$A_E \equiv A_E a_r \quad (15a)$$

$$A_H \equiv A_H a_r \quad (15b)$$

From Eqs. (12a) and (13a) it is clear that Eqs. (15a) and (15b) result in waves with only transverse magnetic and transverse electric fields, respectively.

The scalar potentials, ϕ_E and ϕ_H , are not independent of the vector potentials A_E and A_H and may be selected arbitrarily. The following selections lead to convenient results:

$$\phi_E \equiv -\frac{1}{j\omega \mu \epsilon} \cdot \frac{\partial A_E}{\partial r} \quad (16a)$$

$$\phi_H \equiv -\frac{1}{j\omega \mu \epsilon} \cdot \frac{\partial A_H}{\partial r} \quad (16b)$$

Expressing Eqs. (14a) and (14b) in spherical coordinates and using (16a) and (16b), the following scalar wave equations are obtained:

$$\nabla^2 \left(\frac{A_E}{r} \right) + k^2 \cdot \left(\frac{A_E}{r} \right) = 0 \quad (17a)$$

$$\nabla^2 \left(\frac{A_H}{r} \right) + k^2 \cdot \left(\frac{A_H}{r} \right) = 0 \quad (17b)$$

Equations (17a) and (17b) are readily solved by the method of separation of variables. For outward traveling waves with the polar axis included in the region,

$$\left(\frac{A_H}{r} \right) = a_{mv} \cdot h_v^{(2)}(kr) \cdot P_v^m(\cos \theta) \cdot \begin{bmatrix} \cos(m\phi) \\ \sin(m\phi) \end{bmatrix} \quad (18a)$$

$$\left(\frac{A_E}{r} \right) = b_{mv} \cdot h_v^{(2)}(kr) \cdot P_v^m(\cos \theta) \cdot \begin{bmatrix} \sin(m\phi) \\ \cos(m\phi) \end{bmatrix} \quad (18b)$$

where a_{mv} , b_{mv} are TM and TE wave amplitudes

$h_v^{(2)}(kr)$ = the fractional order, outward spherical Hankel function (Refs. 5 and 6)

$P_v^m(\cos \theta)$ = fractional degree associated Legendre function of the first kind (Refs. 5, 7)

Equations (18b), (12a) and (11a) can be used to find the expressions for the TM field components, and Eqs. (18a), (13a) and (11b) can be used to obtain the TE field components. The resulting expressions, previously published by Borgnis and Papas (Ref. 8) are the appropriate expressions for the fields in an infinite, smooth wall conical waveguide. For anisotropic impedance walls, as in a hybridmode horn, hybrid modes may be defined which are combinations of TM and TE modes. Thus, the HYBRIDHORN fields are expressed as:

$$E_{rmn} = +E_{mn} \cdot v_n \cdot (v_n + 1) \cdot \frac{h_v^{(2)}(kr)}{kr} \cdot P_v^m(\cos \theta) \cdot \sin(m\phi) \quad (19a)$$

$$H_{rmn} = - \left(\frac{E_{mn}}{Z_0} \right) \cdot \text{BAL}_{mn} \cdot v_n \cdot (v_n + 1) \cdot \frac{h_v^{(2)}(kr)}{kr} \cdot P_v^m(\cos \theta) \cdot \cos(m\phi) \quad (19b)$$

$$E_{\theta mn} = -jE_{mn} \cdot \left\{ \frac{j}{kr} \cdot \frac{\partial}{\partial r} [rh_v^{(2)}(kr)] \cdot \frac{\partial P_v^m(\cos \theta)}{\partial \theta} + \text{BAL}_{mn} \cdot m \cdot h_v^{(2)}(kr) \frac{P_v^m(\cos \theta)}{\sin \theta} \right\} \cdot \sin(m\phi) \quad (19c)$$

$$E_{\phi mn} = -jE_{mn} \cdot \left\{ \frac{jm}{kr} \cdot \frac{\partial}{\partial r} [rh_v^{(2)}(kr)] \cdot \frac{P_v^m(\cos \theta)}{\sin \theta} + \text{BAL}_{mn} \cdot h_v^{(2)}(kr) \cdot \frac{\partial P_v^m(\cos \theta)}{\partial \theta} \right\} \cdot \cos(m\phi) \quad (19d)$$

$$H_{\theta mn} = +j \left(\frac{E_{mn}}{Z_0} \right) \cdot \left\{ m \cdot h_v^{(2)}(kr) \cdot \frac{P_v^m(\cos \theta)}{\sin \theta} + \frac{j \text{BAL}_{mn}}{kr} \cdot \frac{\partial}{\partial r} [rh_v^{(2)}(kr)] \cdot \frac{\partial P_v^m(\cos \theta)}{\partial \theta} \right\} \cdot \cos(m\phi) \quad (19e)$$

$$H_{\phi mn} = -j \left(\frac{E_{mn}}{Z_0} \right) \cdot \left\{ h_{\nu}^{(2)}(kr) \cdot \frac{\partial P_{\nu}^m(\cos \theta)}{\partial \theta} + j \text{BAL}_{mn} \cdot \frac{m}{kr} \cdot \frac{\partial}{\partial r} [rh_{\nu}^{(2)}(kr)] \cdot \frac{P_{\nu}^m(\cos \theta)}{\sin \theta} \right\} \cdot \sin(m\phi) \quad (19)$$

With the assumed circumferential grooves, the boundary conditions are:

$$E_{\phi} \Big|_{\theta=\theta_1} = 0 \quad (20)$$

$$\frac{H_{\phi}}{E_r} \Big|_{\theta=\theta_1} = \text{longitudinal wall admittance} \equiv Y_m(kr) \quad (21)$$

which results in,

$$\sum_{n=1}^{n=\infty} E_{mn} \cdot \left\{ \frac{j m}{kr} \cdot \frac{\partial}{\partial r} [rh_{\nu}^{(2)}(kr)] \cdot \frac{P_{\nu}^m(\cos \theta_1)}{\sin \theta_1} + \text{BAL}_{mn} \cdot h_{\nu}^{(2)}(kr) \cdot \frac{\partial P_{\nu}^m(\cos \theta)}{\partial \theta} \Big|_{\theta=\theta_1} \right\} = 0 \quad (22)$$

and

$$Y_m(kr) = -\frac{j}{Z_0} \frac{\sum_{n=1}^{n=\infty} E_{mn} \cdot \left\{ h_{\nu}^{(2)}(kr) \cdot \frac{\partial P_{\nu}^m(\cos \theta)}{\partial \theta} \Big|_{\theta=\theta_1} + j \text{BAL}_{mn} \cdot \frac{m}{kr} \cdot \frac{\partial}{\partial r} [rh_{\nu}^{(2)}(kr)] \cdot \frac{P_{\nu}^m(\cos \theta_1)}{\sin \theta_1} \right\}}{\sum_{n=1}^{n=\infty} E_{mn} \cdot \nu_n \cdot (\nu_n + 1) \cdot \frac{h_{\nu}^{(2)}(kr)}{kr} \cdot P_{\nu}^m(\cos \theta_1)} \quad (23)$$

The technique of separating variables, which allowed expression of Eqs. (17a) and (17b) as two sets of three total differential equations with solutions as Eqs. (18a) and (18b), requires that Eqs. (22) and (23) be satisfied for all values of kr in the horn. The spherical Hankel function $h_{\nu}^{(2)}(kr)$ and the radial derivative function, $\partial/\partial r [rh_{\nu}^{(2)}(kr)]$ are both complex and bear a differing relationship to each other as a function of kr . It is thus clear that Eq. (22) cannot be satisfied by a single HE_{mn} or EH_{mn} mode, but rather a summation of modes must be used, as shown. The literature contains an extensive discussion of this problem (Refs. 9 and 10). Clearly, some approximation must be invoked to arrive at the single mode characteristic equation analogous to (7) and the balance condition analogous to (5). The approximations appearing in the literature are both numerically unjustified and lead to equations which cannot be directly compared to the small flare angle formulation discussed in the previous section.

A neat solution to the above dilemma is obtained by using a result derived by Ludwig (Ref. 4). Ludwig showed that if

$$h_{\nu}^{(2)}(kr) \equiv |h_{\nu}^{(2)}(kr)| e^{-j\alpha_{\nu}(kr)} \quad (24)$$

then

$$\bar{\beta}_{mn} = \frac{\partial \alpha_{\nu}(kr)}{\partial (kr)} = \frac{1}{|(kr) \cdot h_{\nu}^{(2)}(kr)|^2} \quad (\text{exact}) \quad (25)$$

Using Eq. (25), it is easily shown that,

$$\frac{1}{kr} \cdot \frac{\partial}{\partial r} [rh_{\nu}^{(2)}(kr)] = h_{\nu}^{(2)}(kr) \cdot (-j\bar{\beta}_{mn} - \text{ERROR}) \quad (26)$$

where

$$\text{ERROR} \equiv \frac{1}{2} \cdot \frac{1}{\bar{\beta}_{mn}} \cdot \frac{\partial \bar{\beta}_{mn}}{\partial (kr)} \quad (27)$$

The normalized propagation constant $\bar{\beta}_{mn}$ differs significantly from unity for typical horn geometries, but the change of $\bar{\beta}_{mn}$ with kr is slow, leading to a small value for the error term. Figure 2 is a plot of $(1 - \bar{\beta}_{mn})$, $|\text{ERROR}|$ and $|\text{ERROR}|/(1 - \bar{\beta}_{mn})$ for kr from 1 to 100 and ν from 1 to 20. The approximation of retaining the nonunity value for $\bar{\beta}_{mn}$, but neglecting the error term, is seen to be excellent; the relative magnitudes of the error and $(1 - \bar{\beta}_{mn})$ terms are seen to decay as approximately $1/(kr)$. Thus, the approximation is made that,

$$\frac{1}{kr} \cdot \frac{\partial}{\partial r} [r h_{\nu}^{(2)}(kr)] \approx -j \bar{\beta}_{mn} \cdot h_{\nu}^{(2)}(kr) \quad (28)$$

Combining Eq. (28) with (19a) and (19b),

$$E_{rmn} = + E_{mn} \cdot \nu_n \cdot (\nu_n + 1) \cdot \frac{h_{\nu}^{(2)}(kr)}{kr} \cdot P_{\nu}^m(\cos \theta) \cdot \sin(m\phi) \quad (29a)$$

$$H_{rmn} = - \left(\frac{E_{mn}}{Z_0} \right) \cdot \text{BAL}_{mn} \cdot \nu_n \cdot (\nu_n + 1) \cdot \frac{h_{\nu}^{(2)}(kr)}{kr} \cdot P_{\nu}^m(\cos \theta) \cdot \cos(m\phi) \quad (29b)$$

$$E_{\theta mn} = -j E_{mn} \cdot h_{\nu}^{(2)}(kr) \cdot \frac{P_{\nu}^m(\cos \theta)}{\sin \theta} \cdot [\bar{\beta}_{mn} \cdot F_{mn}(\cos \theta) + m \cdot \text{BAL}_{mn}] \cdot \sin(m\phi) \quad (29c)$$

$$E_{\phi mn} = -j E_{mn} \cdot h_{\nu}^{(2)}(kr) \cdot \frac{P_{\nu}^m(\cos \theta)}{\sin \theta} \cdot [m \cdot \bar{\beta}_{mn} + \text{BAL}_{mn} \cdot F_{mn}(\cos \theta)] \cdot \cos(m\phi) \quad (29d)$$

$$H_{\theta mn} = +j \left(\frac{E_{mn}}{Z_0} \right) \cdot h_{\nu}^{(2)}(kr) \cdot \frac{P_{\nu}^m(\cos \theta)}{\sin \theta} \cdot [m + \bar{\beta}_{mn} \cdot \text{BAL}_{mn} \cdot F_{mn}(\cos \theta)] \cdot \cos(m\phi) \quad (29e)$$

$$H_{\phi mn} = -j \left(\frac{E_{mn}}{Z_0} \right) \cdot h_{\nu}^{(2)}(kr) \cdot \frac{P_{\nu}^m(\cos \theta)}{\sin \theta} \cdot [F_{mn}(\cos \theta) + m \cdot \bar{\beta}_{mn} \cdot \text{BAL}_{mn}] \cdot \sin(m\phi) \quad (29f)$$

where

$$F_{mn}(\cos \theta) \equiv \frac{\frac{\partial P_{\nu}^m(\cos \theta)}{\partial \theta}}{\frac{P_{\nu}^m(\cos \theta)}{\sin \theta}} \quad (30)$$

A comparison of Eqs. (29a) to (29f) with Eqs. (1a) to (1f) shows that the approximation in Eq. (28) yields expressions for the fields in a large flare angle horn which are identical in form to those for the small flare angle (Bessel) formulation. The mathematical equivalence between the associated Legendre function and the Bessel function is covered by Ludwig (Ref. 4). Direct numerical comparisons between the two formulations will be discussed in the following section.

With the approximation in Eq. (28), the horn boundary conditions may now be satisfied individually by each mode, and result in the following relationships:

$$\text{BAL}_{mn} = - \frac{m \cdot \bar{\beta}_{mn}}{F_{mv}(\cos \theta_1)} \quad (31)$$

$$Y_m(kr) = - \left(\frac{j}{Z_0} \right) \cdot \frac{1}{\nu_n(\nu_n + 1)} \cdot \frac{kr}{\sin \theta_1} \cdot [F_{mv}(\cos \theta_1) + m \cdot \bar{\beta}_{mn} \cdot \text{BAL}_{mn}] \quad (32)$$

Equation (32) implies that the wall admittance must be a specified function of kr . The amount of mode conversion which would occur with constant depth grooves in the horn flare has not been investigated but, based on previous experimental results, is expected to be small. In the HYBRIDHORN program, a constant groove depth and the radial line impedance formula (Eq. 8) are assumed. With the relationship

$$Y_m(kr) = - \left(\frac{j}{Z_0} \right) \cdot \frac{S_m(x'_1, x'_0)}{(kr) \theta_1} \quad (33)$$

The characteristic equation is obtained from (31) and (32) as:

$$F_{mv}^2(\cos \theta_1) - m^2 \cdot \bar{\beta}_{mn}^2 - \frac{\nu_n \cdot (\nu_n + 1)}{(kr)^2} \cdot \left(\frac{\sin \theta_1}{\theta_1} \right) \cdot F_{mv}(\cos \theta_1) \cdot S_m(x'_1, x'_0) = 0 \quad (34)$$

The upgraded HYBRIDHORN program allows computations to be performed using either the small flare angle (Bessel) formulation, given in Section I above, or the large flare angle (Legendre) formulation, given in this section. The following section discusses numerical results.

III. Numerical Results and Conclusions

The upgraded HYBRIDHORN program allows user selection of either small flare angle (Bessel) or large flare angle (Legendre) computations. The former involve less machine time and are thus normally preferable. For the dominant HE_{11} mode, direct comparisons were made as a function of flare angle. Table I gives the horn geometrical parameters and the results of this comparison. The general conclusion is that the Bessel (small flare angle) option may be safely used for horn flare angles less than 20 degrees. Numerical experiments for a 20 degree flare angle were also performed for higher-order modes, azimuthal variations from $m = 0$ to $m = 3$, and for both smooth and corrugated horn walls; a similar conclusion was obtained from these experiments.

The relative pattern insensitivity to formulation selection is a somewhat negative and surprising result, but does lend great confidence to the correctness of both formulations, and also settles the question of whether the Bessel (old) formulation is sufficiently accurate for typical DSN feedhorn configurations.

In the process of upgrading the HYBRIDHORN program to handle both formulations and the case of $m \neq 1$, the coding was generally improved, including conversion of all major program elements to structured Fortran (SFTRAN, version 2). This coding improvement should facilitate future program maintenance.

References

1. P. D. Potter, "Efficient Antenna Systems: A New Computer Program for the Design and Analysis of High-Performance Conical Feedhorns," *JPL Technical Report 32-1526*, Vol. XIII, pp. 92-107, Jet Propulsion Laboratory, Pasadena, Calif., February 15, 1973.
2. M. S. Narasimhan and B. V. Rao, "Hybrid Modes in Corrugated Conical Horns," *Electronic Letters*, Vol. 6, No. 2, pp. 32-34, Jan. 22, 1970.
3. P. J. B. Clarricoats and P. K. Saha, "Propagation and Radiation Behavior of Corrugated Feeds - Part 1: Corrugated Waveguide Feed," *Proc. IEE (British)*, Vol. 118, No. 9, pp. 1167-1176, Sept. 1971.
4. A. Ludwig, "Antennas for Space Communications: Antenna Feed Research," in *Supporting Research and Advanced Development, Space Programs Summary 37-22*, Vol. IV, pp. 184-189, Jet Propulsion Laboratory, Pasadena, Calif., Aug. 31, 1963.
5. J. A. Stratton, *Electromagnetic Theory*, Chapter 7, McGraw-Hill Book Company, Inc., New York, 1941.
6. *Handbook of Mathematical Functions*, Chapter 10, Milton Abramowitz and Irene A. Stegun, Eds., National Bureau of Standards, GPO, Washington, D.C., June, 1964.
7. *Ibid.*, Chapter 8.
8. F. E. Borgnis and C. H. Papas, "Electromagnetic Waveguides," in S. Flugge, *Handbuch der Physik*, Vol. XVI, pp. 352-358, Springer-Verlag, Berlin, 1958.
9. P. J. B. Clarricoats and P. K. Saha, "Propagation and Radiation Behavior of Corrugated Feeds - Part 2: Corrugated-Conical-Horn Feed," *Proc. IEE (British)*, Vol. 118, No. 9, pp. 1177-1186, Sept. 1971.
10. M. E. J. Jeukens and C. W. Lambrechtse, "Small Corrugated Conical-Horn Antenna with Wide Flare Angle," *Electronic Letters*, Vol. 5, pp. 489-490, October 2, 1969.

Table 1. HE₁₁ mode flare angle comparisons*

| Flare Angle | β_{11} (Aperture cap) | | BAL ₁₁ (Aperture cap) | | $F_m(\theta_1), F_{m\nu}(\cos \theta_1)$ (Aperture cap) | | K_{11} (Aperture cap) | | Bessel pattern error relative to Legendre at -40 dB level, dB |
|-------------|--------------------------------|----------|-------------------------------------|----------|--|----------|----------------------------|----------|--|
| | Bessel | Legendre | Bessel | Legendre | Bessel | Legendre | Bessel | Legendre | |
| 20° | .99969 | .99969 | 1.06386 | 1.06347 | -.93968 | -.94003 | .11102 | .11191 | 0.1 |
| 40° | .99973 | .99971 | 1.05999 | 1.05848 | -.94315 | -.94448 | .10439 | .10748 | 0.3 |
| 60° | .99978 | .99975 | 1.05386 | 1.05072 | -.94869 | -.95149 | .09385 | .10024 | 0.7 |
| 70° | .99981 | .99977 | 1.05008 | 1.04602 | -.95213 | -.95579 | .08734 | .09559 | 1.0 |

*Frequency = 8.415 GHz
Aperture diameter = 106.68 cm (42 in.)
Groove depth = 5.0927 cm (2.005 in.)

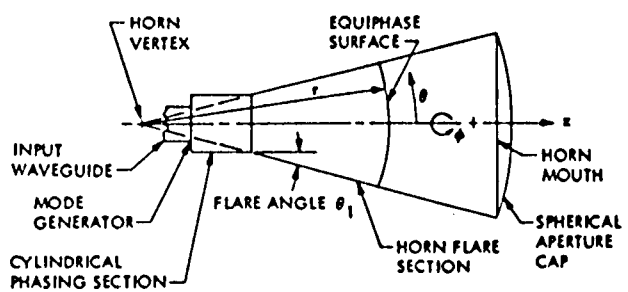


Fig. 1. Horn geometry

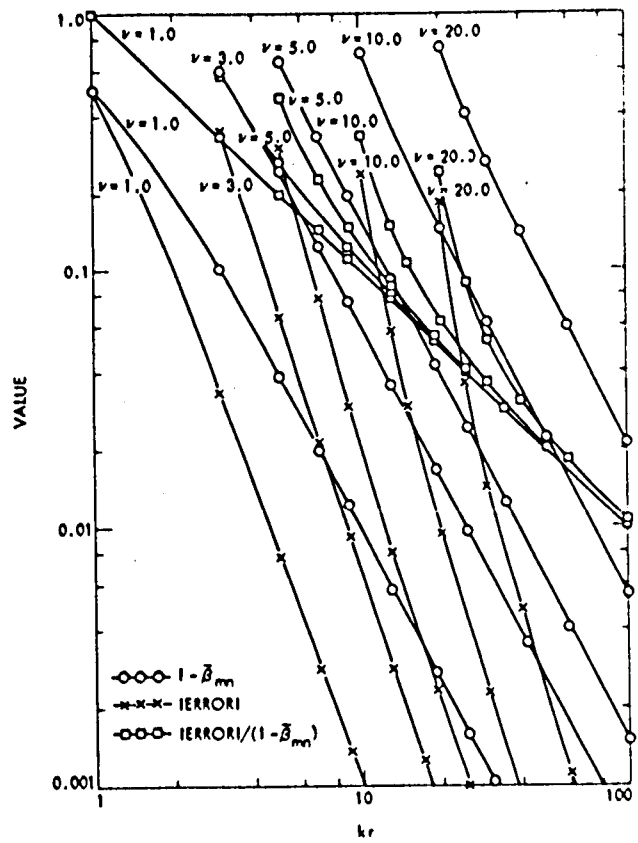


Fig. 2. Large flare angle approximation errors